Available online at www.sciencedirect.com
SCIENCE DIRECT®
Acta Materialia 53 (2005) 3689–3694
Acta MATERIALIA
www.actamat-journals.com

Engineering nanophase self-assembly with elastic field

Wei Lu *, Dongchoul Kim

Department of Mechanical Engineering, University of Michigan, 2250 GGBrown Building, 2350 Hayward Street, Ann Arbor, MI 48109, United States

Received 19 March 2005; received in revised form 11 April 2005; accepted 13 April 2005
Available online 31 May 2005

Abstract

A binary monolayer on an elastic substrate may separate into two phases, which self-assemble into ordered nanoscale patterns. We apply an elastic field to the substrate to guide the self-assembly process. The effect of arbitrary three-dimensional external loading is found to be characterized by a single two-dimensional parameter – a surface stain field of the substrate. A non-uniform strain field significantly influences the size, shape and orientation of self-assembled features, and may induce the formation of pattern colonies. It is shown that a pattern orientates normal to the strain gradient direction. An applied load anchors the position of a self-assembled pattern relative to the substrate, where a colony boundary resides on the strain gradient region. The work suggests a method of strain field design to make various monolayer patterns for nanofabrication.

Keywords: Self-organization and patterning; Nanostructure; Phase-field models; Spinodal decomposition

1. Introduction

Self-organized monolayers have received considerable attention in recent years for their potential in nanofabrication. Experiments have shown that a binary monolayer on an elastic substrate may separate into two phases, which self-assemble into ordered patterns. Examples include triangular lattice of dots, parallel stripes or serpentine stripes [1–5]. The feature size is on the order of 1–100 nm, and often stable on annealing. Recall that when a bulk two-phase alloy is annealed, the phases will coarsen to reduce the total area of the phase boundary. For a two-phase monolayer on a solid surface, the phase boundaries are lines with excess energy, which also drive phase coarsening. The observed stable feature size suggests that, in addition to the phase coarsening action, a phase refining action must exist. The concentration-dependent surface stress can provide such an action [6–11]. The two phases have different surface stresses, leading to a resultant line force at the phase boundary. This induces a fringe elastic field in the substrate, whose depth scales with the phase size. The smaller the two phases, the lower the elastic energy. The competition between the phase boundary energy and the elastic energy selects an equilibrium phase size. The work of Vanderbilt and co-workers [6–8] and Marchenko [12] highlighted the competing effects of the long range elastic interaction and the phase boundary energy. However, the sharp interface leads to a singular elastic field. The pre-assumption of the pattern types excludes many possible configurations. We have recently developed diffuse interface models to study monolayer self-assembly [9–11], where the phase boundary is represented by a concentration gradient, an approach analogous to the work of Cahn and Hilliard [13] on spinodal decomposition. Our model is dynamic, allowing phases and interfaces to emerge and dissolve naturally. A monolayer can self-assemble into whatever pattern it favors. In the diffuse interface framework, the effects of surface stress anisotropy [14], substrate elastic anisotropy [15], surface chemistry [16] and multiple phases [17] have been studied. Order parameters have also been extended to the study [18].

* Corresponding author. Tel.: +1 734 647 7858; fax: +1 734 647 3170.
E-mail address: weilu@umich.edu (W. Lu).

1359-6454/$30.00
doi:10.1016/j.actamat.2005.04.021

Previous researches focused on understanding the self-assembly process due to the intrinsic monolayer–substrate interaction. It is of both scientific and technical interest to investigate how external loading on the substrate affects the pattern formation. The study may lead to novel methods to engineer nanophase self-assembly. In practice, there are many ways to induce an elastic field in the substrate. In addition to direct mechanical loading, pre-patterning a substrate with different materials by photolithography or applying an electric field to a substrate embedded with piezoelectric particles produce diverse well-defined strain fields. Both compressive and tensile strains have been achieved in experiments [19–21].

In this paper, we show that the effect of arbitrary three-dimensional external loading on monolayer self-assembly is characterized by a single two-dimensional surface strain field of the substrate. A non-uniform strain field significantly influences the size, shape and orientation of self-assembled features.

2. A model of monolayer self-assembly guided by external loading

To consider the effect of external loading, it is necessary to distinguish two loading modes: displacement and force. An illustration is given in Fig. 1. With displacement loading, the substrate is stretched or compressed on a surface A_u by a displacement $\bar{u}_i$ and then fixed. With force loading, a distributed force $\bar{t}_i$ is applied on a surface A_t and a distributed body force $\bar{f}_{B_i}$ is applied in the substrate. Note that $\bar{u}_i, \bar{t}_i$ and $\bar{f}_{B_i}$ are functions of position and can vary from point to point. The two loading modes affect self-assembly differently. By the monolayer–substrate interaction, the pattern evolution causes redistribution of strain field in the substrate. This will not cause any external work through A_u since it is fixed. However, the strain evolution causes displacements of material points in the substrate and on A_t. Thus the force loading $\bar{f}_{B_i}$ and $\bar{t}_i$ will do work, which changes the system energy and in turn affects the evolution. Note that in addition to other surfaces, the top surface may be subjected to an external load. In this special case the force boundary A_t also involves the top surface.

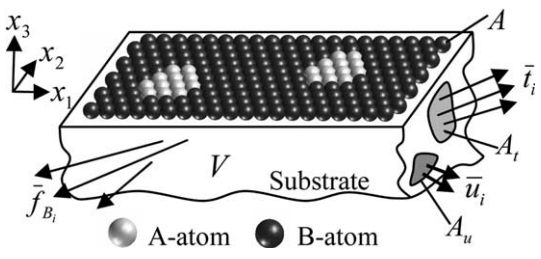

Fig. 1. Schematic of self-organized nanoscale patterns on a substrate.

Imagine a monolayer of two atomic species, A and B, which forms a coherent lattice with the substrate. Two kinds of atoms prefer to form bonds with the substrate, rather than pile up into islands. Thus, the diffusion is restricted within the monolayer. We model the monolayer as an infinitely large surface and the substrate a semi-infinite elastic body. The substrate occupies the half space $x_3 < 0$ and is bounded by the x_1–x_2 plane, as shown in Fig. 1. The free energy of the system comprises the surface energy in the monolayer, the elastic energy in the substrate and external work, namely

$$G = \int_V W \, \mathrm{d}V + \int_A \Gamma \, \mathrm{d}A - \int_V \bar{f}_{B_i} u_i \, \mathrm{d}V - \int_{A_t} \bar{t}_i u_i \, \mathrm{d}A. \tag{1}$$

The first integral extends over the volume of the entire system, W being the elastic energy per unit volume. The second integral extends over the top surface A, where Γ is the surface energy per unit area. The last two terms account for the external forces and u_i is the displacement. A repeated index implies summation. Both the volume and the surface are measured in the unstrained substrate. Note that other than the top surface, other surfaces do not involve in diffusion. Their contribution to the surface energy is constant and thus excluded from Eq. (1).

The elastic energy per unit volume in the bulk, $W = c_{ijkl}\varepsilon_{ij}\varepsilon_{kl}/2$, is a quadratic function of strain ε_{ij}, with c_{ijkl} being the elastic stiffness. The monolayer is a substitutional alloy. Let concentration C be the fraction of atomic sites on the surface occupied by species B, and regard it as a time-dependent, spatially continuous function $C(x_1,x_2,t)$. Assume that Γ is a function of the concentration C, the concentration gradient $\partial C/\partial x_\alpha$ and the strain in the surface $\varepsilon_{\alpha\beta}$. A Greek subscript runs from 1 to 2. Expand $\Gamma(C,\partial C/\partial x_\alpha,\varepsilon_{\alpha\beta})$ into the leading-order terms in the concentration gradient $\partial C/\partial x_\alpha$ and the strain $\varepsilon_{\alpha\beta}$, we obtain

$$\Gamma = g + h(\nabla C)^2 + f_{\alpha\beta}\varepsilon_{\alpha\beta}, \tag{2}$$

where g, h and $f_{\alpha\beta}$ are all functions of the concentration C, and $(\nabla C)^2 = (\partial C/\partial x_1)^2 + (\partial C/\partial x_2)^2$. We have assumed that h is isotropic. The leading-order term in the concentration gradient is quadratic because, by symmetry, the linear term does not affect the surface energy. We have neglected terms quadratic in the strain, which relate to the excess in the elastic stiffness of the epilayer relative to the substrate.

When the concentration field is uniform and the substrate is unstrained, $g(C)$ is the only remaining term in Eq. (2). Hence, $g(C)$ represents the surface energy per unit area of a uniform monolayer on an unstrained substrate. To describe phase separation, we may prescribe $g(C)$ as any function with double wells. In this letter, to be definite, we assume a regular solution

$$g(C) = g_A(1-C) + g_B C + \Lambda k_b T[C\ln C + (1-C) \times \ln(1-C) + \Omega C(1-C)], \quad (3)$$

where g_A and g_B are the chemical potentials of pure A and B on the substrate surface. The first two terms in the bracket result from the entropy of mixing, and the third term from the enthalpy of mixing. Λ is the number of atoms per unit area on the surface, k_b the Boltzmann's constant, and T the absolute temperature. The dimensionless number Ω measures the bond strength relative to the thermal energy $k_b T$. When $\Omega > 2$, the function g has double wells and drives phase separation. The second term in Eq. (2) represents the phase boundary energy, which drives phase coarsening. We assume that $h(C) = h_0$ is a positive constant. Any non-uniformity in the concentration field by itself increases Γ. The quantity $f_{\alpha\beta}$, known as surface stress, is the surface energy change associated with the elastic strain [22,23]. It drives phase refining [9–11]. As a first-order consideration, we interpolate $f_{\alpha\beta}(C)$ linearly by the surface stress of pure A and B monolayer. The form of $f_{\alpha\beta}(C) = \psi_{\alpha\beta} + \phi_{\alpha\beta}C$, where $\psi_{\alpha\beta}$ and $\phi_{\alpha\beta}$ are material constants, is also consistent with experiments [23].

Atoms diffuse within the epilayer to reduce the free energy of the system expressed by Eq. (1). The energy variation associated with mass relocation defines the driving force for diffusion. The energy variation associated with displacement gives the elastic equilibrium equation. Following an approach similar to that in [10,11], we obtain:

$$\frac{\partial C}{\partial t} = \frac{M}{\Lambda^2}\nabla^2\left(\frac{\partial g}{\partial C} - 2h_0\nabla^2 C + \phi_{\alpha\beta}\varepsilon^m_{\alpha\beta} + \phi_{\alpha\beta}\varepsilon^e_{\alpha\beta}\right), \quad (4)$$

where M is the mobility of atoms in the monolayer and $\nabla^2 = \partial^2/\partial x_1^2 + \partial^2/\partial x_2^2$. $\varepsilon^m_{\alpha\beta}$ and $\varepsilon^e_{\alpha\beta}$ are the strains due to intrinsic monolayer–substrate interaction and external loading, respectively. For simplicity, we have adopted a common practice of assuming a constant mobility [10,11,14–18]. Generally speaking, the mobility may depend on local concentration and strain. The dependence on strain can be neglected since the strain involved is small. The diffusion within the monolayer proceeds by an atomic exchange mechanism. The mobility has a strong dependence on the local structure and thus the concentration C. Recent studies show that for some specific $M(C)$, the concentration dependence is actually irrelevant for the asymptotic behavior. A variable mobility may influence the rate of phase growth, but the phase patterns are similar [24]. Particularly, in our model the concentration-dependent surface stress provides a refining action against coarsening, leading to an equilibrium phase size. The concentration dependence of mobility seems to be irrelevant for the present purpose. Nevertheless the kinetics with a variable mobility is an interesting topic worth further pursuing.

The elastic field in the substrate due to the intrinsic monolayer–substrate interaction is determined by

$$\frac{\partial \sigma^m_{ij}}{\partial x_j} = 0 \quad (5)$$

in the bulk with boundary conditions:

$$\sigma^m_{3\alpha} = \frac{\partial f_{\alpha\beta}}{\partial x_\beta} = \phi_{\alpha\beta}\frac{\partial C}{\partial x_\beta}, \quad \sigma^m_{33} = 0 \text{ on } x_3 = 0 \text{ surface.} \quad (6)$$

The surface strain $\varepsilon^m_{\alpha\beta}(x_1, x_2)$ is obtained by solving the above elastic problem. Note that the concentration enters the elastic field through the boundary conditions: a non-uniform concentration field generates a shear force on the substrate. To focus on the effect of external loading, we consider an isotropic material system. The material constants are Young's modulus E, Poisson's ratio ν, $\phi_{11} = \phi_{22} = \phi$ and $\phi_{12} = 0$. The situation is close to the self-assembly on the (1 1 1) surface of many body-centered cubic or face-centered cubic crystals. The elastic field in an isotropic half space due to a tangential point force acting on the surface was solved by Cerruti [25]. The expression for $\varepsilon^m_{\alpha\alpha}$ can be obtained by integrating the point force solution, giving

$$\varepsilon^m_{\alpha\alpha} = -\frac{(1-\nu^2)\phi}{\pi E}\int\int \frac{(x_1-\xi_1)\frac{\partial C}{\partial \xi_1} + (x_2-\xi_2)\frac{\partial C}{\partial \xi_2}}{\left[(x_1-\xi_1)^2 + (x_2-\xi_2)^2\right]^{3/2}} \, d\xi_1 \, d\xi_2. \quad (7)$$

The external loading generates an elastic field in the substrate, which is determined by

$$\frac{\partial \sigma^e_{ij}}{\partial x_j} + \bar{f}_{B_i} = 0 \quad (8)$$

in the bulk with boundary conditions:

$$\sigma^e_{ij} n_j = \bar{t}_i \text{ on } A_t, \quad u_i = \bar{u}_i \text{ on } A_u. \quad (9)$$

While this elastic field is three-dimensional, its effect on monolayer diffusion is characterized by a two-dimensional surface strain $\varepsilon^e_{\alpha\beta}(x_1, x_2)$ as shown in Eq. (4). The surface strain $\varepsilon^e_{\alpha\beta}$ can be obtained by solving the elastic problem in the substrate and evaluating the strain field at $x_3 = 0$. Eqs. (8) and (9) involve only external forces and constraints, therefore $\varepsilon^e_{\alpha\beta}$ is independent of concentration. The physical meaning of $\varepsilon^m_{\alpha\beta}$ and $\varepsilon^e_{\alpha\beta}$ is different. The strain $\varepsilon^m_{\alpha\beta}$ is a "passive" strain accompanying the self-assembly process that resists the relaxation of the monolayer, while $\varepsilon^e_{\alpha\beta}$ is a loading parameter. It is key that the details of loading modes, elastic anisotropy, and field distribution in the substrate are reduced to a single parameter. External loads producing identical $\varepsilon^e_{\alpha\beta}$ have the same effect on self-assembly. Eq. (4) reveals that a uniform $\varepsilon^e_{\alpha\beta}$ does not affect diffusion, in contrast to the well-studied morphological changes, where a uniform strain field does drive diffusion. The first two terms in Eq. (3) are linear in concentration. Their contribution

to $\partial g/\partial C$ is g_B–g_A. It is observed in Eq. (4) that $\phi_{\alpha\beta}\varepsilon^e_{\alpha\beta}$ plays the same role as g_B–g_A. Thus, $\varepsilon^e_{\alpha\beta}$ essentially affects diffusion by modifying the chemical potential difference.

A dimensionless parameter measuring the strength of external loading is defined by $R = \phi_{\alpha\beta}\varepsilon^e_{\alpha\beta}/\Lambda k_b T$. R can be positive or negative. A region with positive R favors the attachment of A-atom and competes with its neighbor for them. If the neighbor has negative R, it favors B-atom and expels A-atom. Then the two regions collaborate with each other to exchange atoms. In both cases, the stain changes the local average concentration and pattern. In addition, a strain field may anchor self-assembled features at specific locations.

A comparison of the first two terms in the parentheses of Eq. (4) defines a length $b = \sqrt{h_0/\Lambda k_b T}$, which scales the phase boundary thickness. The magnitude of h_0 is on the order of energy per atom at a phase boundary. Using magnitudes $h_0 \sim 10^{-19}$ J, $\Lambda \sim 5\times10^{19}$ m^{-2} and $k_b T \sim 5\times10^{-21}$ J, we have $b \sim 0.6$ nm. Another length, $l = Eh_0/[\phi^2(1-\nu^2)]$, is defined by comparing the second and third terms in the parenthesis. This length reflects the competition of surface stress and phase boundary. The equilibrium phase size is on the order $\sim 4\pi l$. Young's modulus of a bulk solid is $E \sim 10^{11}$ N/m^2. A representative value for ϕ is $\sim$4 N/m [23]. These parameters give $4\pi l \sim 8$ nm, which broadly agrees with observed sizes. The strength of external loading is $R = \phi\varepsilon^e_{\alpha\alpha}/\Lambda k_b T$. A magnitude of $\varepsilon^e_{\alpha\alpha} = 0.1\%$ gives $R \sim 0.016$. The time scale is $\tau = h_0/[M(k_b T)^2]$. After normalization by the length b and the time τ, Eq. (4) can be solved efficiently in Fourier space [11].

3. Simulations of guided self-assembly

The simulations are taken with material parameters $\Omega = 2.2$, $\nu = 0.3$, $b/l = 1$ and calculation size of $256b \times 256b$. The initial conditions are random: the concentration fluctuates randomly within 0.001 from the average. The boundary conditions are periodic. The concentration field is visualized by gray scale graphs in the (x_1, x_2) plane with darker shade for higher concentration (B-rich). Fig. 2 shows selected results at $t = 5.0\times10^5\tau$ for an average concentration of 0.3. The monolayer separates into two phases. The B-rich phase forms dots embedded in the matrix of A-rich phase. The R-map illustrates the distribution of $R(x_1, x_2)$ within the calculation cell. Fig. 2(a) shows that a monolayer evolves into a multi-domained triangular lattice of dots when R is uniform. The R-map for Fig. 2(b) comprises two stripes: black for $R = 0.01$ (i.e., $\varepsilon^e_{\alpha\alpha} = 6.25\times10^{-4}$) and white for $R = 0$. The monolayer evolves into pattern colonies. The dots form an almost perfect triangular lattice within each colony, and line up with the close packed direction parallel to the edge of the stripes. The lattice in different R region is self-contained, maintaining its own lattice spacing. The R-map for Fig. 2(c) comprises three black curves of $R = 0.1$, with $R = 0$ in the white region. The dots orientate themselves along the wavy edges of the three curves. The narrow curves preclude the formation of any dots inside.

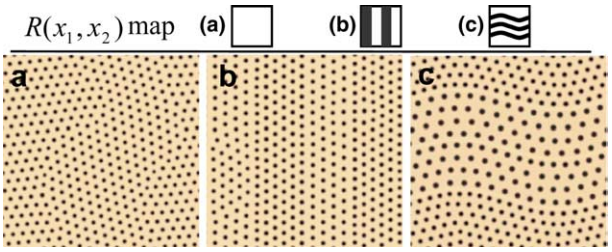

Fig. 2. Various patterns at $t = 5.0\times10^5\tau$ for an average concentration of 0.3. In the R-map the white region has $R = 0$. The black region has (b) $R = 0.01$ (c) $R = 0.1$.

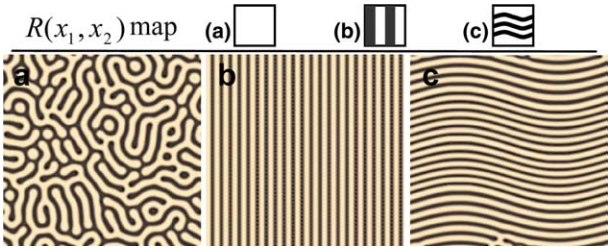

Fig. 3. Various patterns at $t = 5.0\times10^5\tau$ for an average concentration of 0.5. In the R-map the white region has $R = 0$. The black region has (b) $R = 0.01$ (c) $R = 0.1$.

Fig. 3 shows selected results at $t = 5.0\times10^5\tau$ for an average concentration of 0.5. The R-map is the same as that in Fig. 2. A uniform R leads to the serpentine structure in Fig. 3(a). The formation of serpentine structure reflects the symmetry of the system. The evolution sequence shows that the phases reach the equilibrium size very fast. From $t = 1000\tau$ to $5.0\times10^5\tau$, the phase size is almost invariant. The late stage of evolution is characterized by the local reorientation and twisting. After a long time of evolution, the serpentine structure does not show any difference from that in Fig. 3(a). An external load can line up the self-assembled features, as shown in Fig. 3(b). Careful observation shows stripe colonies, similar to what happens in Fig. 2(b). Fig. 3(c) shows the formation of wavy stripes orientating along the strain edges in the R-map. These results suggest that external loading can effectively change size, shape and orientation of self-assembled stripes.

4. Analysis of pattern colony formation

Further analysis of the simulation results reveals the colony formation mechanism and suggests a quantitative relation between the lattice spacing and the loading

parameter $\varepsilon^{e}_{\alpha\alpha}$. The combination of Eqs. (1) and (2) and the elastic equations gives the free energy

$$G = G_0(\bar{f}_{B_i}, \bar{t}_i, \bar{u}_i) + \int_A \left[g + h_0(\nabla C)^2 + \frac{1}{2}\phi_{\alpha\beta}\varepsilon^{m}_{\alpha\beta} C \right] \mathrm{d}A + \int_A \phi_{\alpha\beta}\varepsilon^{e}_{\alpha\beta} C \, \mathrm{d}A, \quad (10)$$

where G_0 is independent of the concentration and thus has no effect on diffusion. The second term comes from the monolayer–substrate interaction, and last term from the interaction between diffusion and external loading. In the following, we consider the free energy of a pattern, and take the triangular lattice of dots as an example.

First, consider the load-free situation. Energy minimization gives the equilibrium pattern. The lattice spacing and average energy per unit area depend on material properties and the average concentration C_0. For a given material system, the spacing and average energy density of the equilibrium state are noted by $b \cdot \tilde{d}(C_0)$ and $\Lambda k_b T \cdot \tilde{g}(C_0)$, where $\tilde{d}$ and $\tilde{g}$ are dimensionless. To compute $\tilde{g}(C_0)$, choose a representative unit shown in Fig. 4. Considering the symmetry about the x_1 and x_2-axis, the concentration is represented by a Fourier series

$$C = C_0 + \sum_m q_{m0} \cos\left(m\frac{2\pi x_1}{\tilde{d}}\right) + \sum_n q_{0n} \cos\left(n\frac{2\pi x_2}{\sqrt{3}\tilde{d}}\right) + \sum_{m,n} q_{mn} \cos\left(m\frac{2\pi x_1}{\tilde{d}}\right)\left(n\frac{2\pi x_2}{\sqrt{3}\tilde{d}}\right), \quad (11)$$

where the summation runs from 1 to ∞. We seek $\tilde{d}$ and the coefficients q_{m0}, q_{0n}, q_{mn} to minimize the free energy. Eqs. (3), (7), (10) and (11) give

$$\tilde{g} = L + \frac{S}{2}\left(\frac{2\pi}{\tilde{d}}\right)^2 - \frac{H}{2}\left(\frac{b}{l}\right)\left(\frac{2\pi}{\tilde{d}}\right), \quad (12)$$

where $L = \int_{-1/2}^{1/2}\int_{-1/2}^{1/2} [C\ln C + (1-C)\ln(1-C) + \Omega C(1-C)]\,\mathrm{d}\xi_1\,\mathrm{d}\xi_2$, $\xi_1 = x_1/\tilde{d}$, $\xi_2 = x_2/\sqrt{3}\tilde{d}$, $S = \sum_m m^2 q_{m0}^2 + \sum_n n^2 q_{0n}^2/3 + 1/2\sum_{m,n}(m^2+n^2/3)q_{mn}^2$, and $H = \sum_m m q_{m0}^2 + \sum_n n q_{0n}^2/\sqrt{3} + 1/2\sum_{m,n}\sqrt{m^2+n^2/3}\,q_{mn}^2$ depend only on the geometry, and not the scale, of the pattern. Setting $\partial\tilde{g}/\partial\tilde{d} = 0$, we obtain the equilibrium size $b\tilde{d} = 4\pi l S/H$. This equation combined with Eq. (12) gives

$$\tilde{g} = L - \frac{1}{8}\left(\frac{b}{l}\right)^2 \frac{H^2}{S}. \quad (13)$$

The equilibrium pattern is parallel stripes when C_0 is close to 0.5. In that case the expression of $\tilde{d}$ (now means the stripe wavelength) and $\tilde{g}$ remains the same, and we only need to retain the q_{m0} summation term in Eq. (11), S and H. We minimize Eq. (13) by the conjugate-gradient method.

Fig. 4 shows the results for dots. Note that the $\tilde{g}$ curve is concave up, so that a uniform triangular lattice will not spontaneously separate into two mesoscale colonies of different lattice spacing; the latter would increase the energy. The pattern in Fig. 2(b) can be explained intuitively by two competing actions. The loading induces opposite movements of A- and B-atom to different R regions, while the formation of colonies increases the energy and resists the diffusion. A stable pattern develops when they reach equilibrium. Fig. 4 also gives the $\tilde{d}$ and d_1/d curve, where d_1 is the dot diameter. We measure d_1 by the 0.5 concentration contour. While $\tilde{d}$ curve is non-monotonic, d_1 increases monotonically in C_0 due to the strong dependence of d_1/d on C_0. The $\tilde{g}$ curve for stripes is very close to that of dots, and has lower energy at $C_0 > 0.4$.

To establish a quantitative relation between the colony lattice and loading, consider a periodic strain of wavelength $l_1 + l_2$, as shown in Fig. 5. The loading parameters are $\varepsilon^{eI}_{\alpha\alpha}$ and $\varepsilon^{eII}_{\alpha\alpha}$. The elastic field induced by the monolayer–substrate interaction decays by $1/r^3$, where r is the distance between two points. It is reasonable to expect that the patterns in two regions are self-contained when the size of each region is much larger than that of the self-assembled features. In fact Fig. 2(b) suggests that the size can be as small as a few lattice spacing. The nice order at the colony boundary also suggests that the

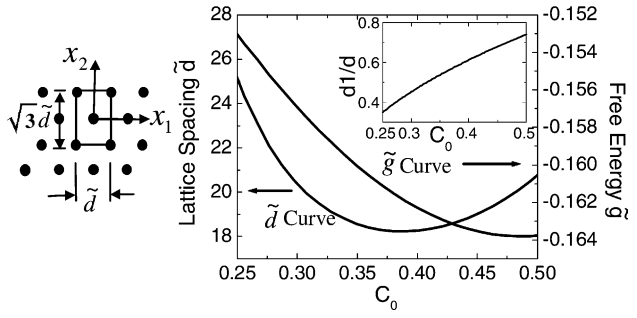

Fig. 4. The equilibrium energy and lattice spacing for a triangular lattice of dots.

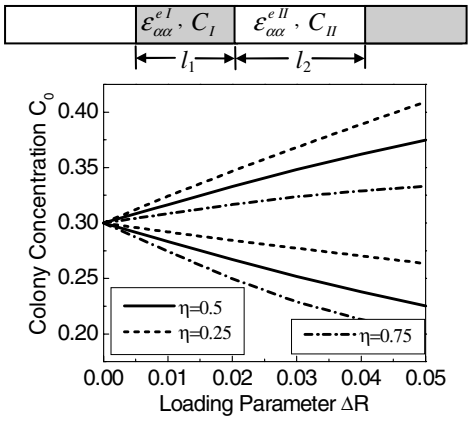

Fig. 5. Relation between the colony concentration and external loading.

colony transition finishes within a lattice spacing. When the size of each strain region is large compared with $\tilde{d}$, Eq. (10) gives a simple expression for the average energy per unit area

$$\frac{g_a}{\Lambda k_b T} = \eta\tilde{g}(C_I) + (1-\eta)\tilde{g}(C_{II}) + \eta C_I \Delta R + C_0 R_2, \quad (14)$$

where C_0 is total average concentration, C_I and C_{II} the average concentration in the l_1 and l_2 region, $\eta = l_1/(l_1 + l_2)$, $\Delta R = \phi\left(\varepsilon^{eI}_{\alpha\alpha} - \varepsilon^{eII}_{\alpha\alpha}\right)/\Lambda k_b T$, and $R_2 = \phi\varepsilon^{eII}_{\alpha\alpha}/\Lambda k_b T$. Mass conservation requires $\eta C_I + (1-\eta)C_{II} = C_0$. The energy minimization by $\partial g_a/\partial C_I = 0$ leads to

$$\tilde{g}'(C_I) - \tilde{g}'(C_{II}) + \Delta R = 0, \quad (15)$$

where $\tilde{g}'$ is the derivative of the function $\tilde{g}$. Eq. (15) reveals the connection between external loading and colony formation. The solution needs Eq. (13) or Fig. 4. Representative results for $C_0 = 0.3$ are given in Fig. 5. External loading induces two colonies of $C_I < C_0$ and $C_{II} > C_0$, as shown by the branching curves. Both ΔR and η affects the colony formation. The difference between C_I and C_{II} increases with ΔR. The two concentrations are almost symmetric about C_0 with $\eta = 0.5$, and shift toward larger concentrations with $\eta = 0.25$ and lower concentrations with $\eta = 0.75$. Define the colony chemical potentials by $\mu_I = \mu_0(C_I) + \phi_{\alpha\beta}\varepsilon^{eI}_{\alpha\beta}$, where $\mu_0(C_I) = \Lambda k_b T \mathrm{d}\tilde{g}(C_I)/\mathrm{d}C_I$ is the load-free colony chemical potential. Eq. (15) shows that two colonies reach equilibrium when they have equal chemical potentials, i.e., $\mu_I = \mu_{II}$. A generalization of this relation gives $\mu_I = \mu_{II} = \cdots = \mu_N$, which can be applied to make a distribution of pattern colonies. Similar analysis applies to stripe colonies.

5. Discussion

The average concentration is well known to affect the pattern types, as can be seen by comparing Figs. 2(a) and 3(a), or from experimental observations [1–5]. Similar stripe and triangular dot patterns have been observed in other systems involving different mechanisms, such as electropolishing [26]. It is of both scientific and technical interest to investigate how external loading on the substrate affects the pattern formation. While it is known from experimental observations that a strain may strongly influence the organization of surface deposits, the model and simulations presented in this paper reveal the mechanism and dynamics. It is shown that the effect of an arbitrary external load is uniquely characterized by a surface stain field $\varepsilon^e_{\alpha\beta}$ on the substrate. A non-uniform $\varepsilon^e_{\alpha\beta}$ significantly affects the size, orientation and distribution of self-assembled features. Specifically, the external loading is essential to the formation of colony patterns. Two colonies reach equilibrium when they have equal chemical potentials, which relate to both the pattern configuration and surface strain. Quantitative relations between the feature size distribution and loading conditions have been established. We have shown that the self-assembled features orientate normal to the strain gradient direction. The applied loading can anchor the position of a self-assembled pattern relative to the substrate, where a colony boundary resides on the loading gradient region. Eq. (10) highlights the separation of intrinsic and external energy, allowing the prediction of general loading effect without scanning the whole parameter space. With its flexibility and possible real-time variation, the external loading is unique in influencing self-assembly.

Acknowledgments

The authors acknowledge financial support from National Science Foundation Career Award No. DMI-0348375.

References

[1] Kern K, Niehus H, Schatz A, Zeppenfeld P, George J, Comsa G. Phys Rev Lett 1991;67:855.
[2] Plass R, Last JA, Bartelt NC, Kellogg GL. Nature 2001;412:875.
[3] Pohl K, Bartelt MC, de la Figuera J, Bartelt NC, Hrbek J, Hwang RQ. Nature 1999;397:238.
[4] Schneider KS, Lu W, Owens TM, Fosnacht DR, Banaszak Holl MM, Orr BG. Phys Rev Lett 2004;93:166104.
[5] Schneider KS, Lu W, Fosnacht DR, Orr BG, Banaszak Holl MM. Langmuir 2004;20:1258.
[6] Alerhand OL, Vanderbilt D, Meade RD, Joanaopoulos JD. Phys Rev Lett 1988;61:1973.
[7] Ng K-O, Vanderbilt D. Phys Rev B 1995;52:2177.
[8] Narasimhan S, Vanderbilt D. Phys Rev Lett 1992;69:1564.
[9] Lu W, Suo Z. Z Metallknd 1999;90:956.
[10] Suo Z, Lu W. J Mech Phys Solids 2000;48:211.
[11] Lu W, Suo Z. J Mech Phys Solids 2001;49:1937.
[12] Marchenko VI. Sov Phys JETP 1981;54:605.
[13] Cahn JW, Hilliard JE. J Chem Phys 1958;28:258.
[14] Lu W, Suo Z. Phys Rev B 2002;65:085401.
[15] Lu W, Suo Z. Phys Rev B 2002;65:205418.
[16] Lu W, Kim D. Nano Lett 2004;4:313.
[17] Kim D, Lu W. Nanotechnology 2004;15:667.
[18] Proville L. Phys Rev Lett 2002;88:046102.
[19] Guyer JE, Barnett SA, Voorhees PW. J Cryst Growth 2000;217:1.
[20] Wallart X, Priester C, Deresmes D, Mollot F. Appl Phys Lett 2000;77:253.
[21] Xie YH et al. Phys Rev Lett 1994;73:3006.
[22] Cammarata RC, Sieradzki K. Annu Rev Mater Sci 1994;24:215.
[23] Ibach H. Surf Sci Rep 1997;29:193.
[24] Zhu J, Chen LQ, Shen J, Teekare V. Phys Rev E 1999;60:3564.
[25] Johnson KL. Contact mechanics. Cambridge: Cambridge University Press; 1985.
[26] Yuzhakov VV, Chang HC, Miller AE. Phys Rev B 1997;56:12608.